NJC

ROYAL SOCIETY OF CHEMISTRY

PAPER

View Article Online
View Journal

Cite this: DOI: 10.1039/d1nj02406j

Finely dispersed CuO on nitrogen-doped carbon hollow nanospheres for selective oxidation of sp^3 C–H bonds†

Shyam Sunder R. Gupta and Mannepalli Lakshmi Kantam *

Received 16th May 2021,
Accepted 24th July 2021

DOI: 10.1039/d1nj02406j

rsc.li/njc

Hollow nanostructured materials are of great importance in heterogeneous catalysis owing to their improved mass transfer and diffusion properties. In this study, we have successfully prepared a novel nanocomposite, CuO supported nitrogen-doped carbon hollow nanospheres (denoted as CuO/N-C-HNSs), by a template protection–sacrifice method employing SiO_2 nanospheres as the sacrificial template. The diverse nitrogen species present in the support anchored the CuO nanoparticles firmly and stabilized them as fine particles having sizes below 10 nm. The as-prepared CuO/N-C-HNSs efficiently catalyze the selective oxidation of sp^3 C–H bonds under mild reaction conditions using *t*-butyl hydroperoxide as the oxidant and water as the green solvent. The strong coordination between CuO and nitrogen species prevents the aggregation as well as leaching of CuO nanoparticles during the catalytic reaction. A wide range of aromatic hydrocarbons were smoothly oxidized into the corresponding products at 80 °C in 20 h affording both conversion and selectivity as high as 99%. The excellent catalytic activity and reusability of CuO/N-C-HNSs can be attributed to the uniformly dispersed CuO sites, hollow nanostructure and the synergistic effect between CuO and nitrogen-doped carbon hollow nanospheres.

1. Introduction

Selective oxidation of sp^3 C–H bonds in hydrocarbons is challenging and is of great importance in the chemical industry, since it enables the production of various value-added products such as alcohols, aldehydes and ketones.[1–5] Initially, noble metal based catalytic systems with excellent performance were explored for C–H oxidation reactions.[6–9] However, the high cost and limited availability of noble metals limit their industrial applications. Therefore, various non-noble metal based catalysts were later developed for the oxidation of C–H bonds.[10–18]

In recent years, nitrogen-doped carbon (N–C) materials have emerged as a promising support for the dispersion of various catalytically active metals because the nitrogen present in the support coordinates strongly with the metals[19] and stabilizes them as fine particles[20–27] or even as single atoms[28–37] and additionally the porous structure affords effective mass transport during the catalytic reaction.[38] Considering these benefits, several N–C based materials were fabricated for the selective oxidation of C–H bonds. In this context, the first N–C based material explored for the oxidation of hydrocarbons using *t*-butyl hydroperoxide (TBHP) as an oxidant was g-C_3N_4 by Li and co-workers in 2011.[39] Afterwards, Ma and co-workers also reported the metal-free oxidation of benzylic C–H bonds using nitrogen-doped graphene in the presence of TBHP.[40] In 2013, Zhang *et al.* carried out the oxidation of hydrocarbons in air catalyzed by palladium nanoparticles supported on nitrogen-doped carbon (Pd@N–C).[41] In 2016 and 2017 Liu and co-workers explored various N–C materials for the dispersion of cobalt nanoparticles and studied their catalytic performance for the oxidation of ethyl benzene.[42–44] In 2018, Lin *et al.* prepared a sulphur doped CoNC catalyst for oxidation of ethylbenzene and achieved 82% conversion and 88% selectivity towards acetophenone.[45] Motivated by the excellent catalytic performance of cobalt, various highly efficient Co–N–C based catalysts were developed for the selective oxidation of C–H bonds.[46–50] Besides cobalt, various other non-noble metals such as Fe,[51,52] Cu[53] and Mn[54] have also been used for the fabrication of N–C based catalysts for C–H bond oxidation.

Multiple heteroatom-doped nanocarbons have also been examined extensively for C–H bond oxidation reactions.[55,56] In this background, Yang *et al.* prepared a nitrogen, phosphorus and sulfur co-doped carbocatalyst for the oxidation of aromatic alkanes.[57] Qin *et al.* prepared a sulfur and nitrogen co-doped carbocatalyst for the selective oxidation of aryl alkanes and demonstrated that the pyrolysis of S, N-containing porous organic polymers in the presence of nano-$CaCO_3$ enhances the sulfur content in the resulting S, N co-doped porous carbon.[58] Recently, Su *et al.* fabricated nitrogen-doped carbon nanotubes

Department of Chemical Engineering, Institute of Chemical Technology, Matunga (E), Mumbai – 400019, Maharashtra, India.
E-mail: lk.mannepalli@ictmumbai.edu.in

† Electronic supplementary information (ESI) available. See DOI: 10.1039/d1nj02406j

and explored its catalytic activity for aerobic oxidation of ethylbenzene into acetophenone and achieved 46% conversion and 72% selectivity for the desired product.[59] Multiple heteroatom-doped nanocarbons exhibit excellent catalytic activity towards oxidation of hydrocarbons due to the formation of an improved electronic structure and multiple active defect sites in the material. However, the fabrication of multiple heteroatom-doped nanocarbons is challenging and involves the use of multiple precursors and corrosive and hazardous reagents.[60,61] Moreover, the addition of several heteroatoms requires harmful unit processes, for example, pyrolysis of toxic sulphides and introduction of toxic ammonia at a higher temperature for doping with sulfur and nitrogen, respectively.[62,63] Therefore, the incorporation of multiple heteroatoms in a carbocatalyst through a feasible process still remains a grand challenge.

Among a wide variety of carbon nanostructures, hollow carbon nano-spheres have several advantages such as a rigid framework structure, high porosity and a high surface-to-bulk ratio. The high surface-to-bulk ratio offers a shortened pathway for the mass transport of reactants and products and exposure of more active sites available for the reaction.[64] In this context, Chen *et al.* developed atomic Fe dispersed nitrogen-doped carbon hollow nanospheres for the oxygen reduction reaction and proposed that the nitrogen doping helps in the dispersion of the active metal on the support.[38] Similarly, in our recently published work, we have demonstrated the fabrication of a novel nanocomposite, CuO supported on nitrogen-doped carbon hollow nanospheres, for oxidative methyl-esterification reactions.[65] Co–N–C and Fe–N–C catalysts have been studied extensively for the oxidation of aromatic hydrocarbons, whereas Cu–N–C catalysts have rarely been explored for C–H oxidation reactions.

Herein, for the first time, we report CuO/N-C-HNS catalyzed highly efficient liquid phase oxidation of C–H bonds using TBHP as the oxidizing agent and water as the green solvent. The nanocomposite, CuO/N-C-HNSs, was fabricated by a template protection–sacrifice method using silica nanospheres as the sacrificial template. The ligand histidine coordinates strongly with the copper precursor and affords the formation of finely dispersed CuO particles on the carbon nanostructure. Additionally, histidine serves the purpose of precursor for N and C elements. The schematic illustration of the fabrication of CuO/N-C-HNSs is presented in Fig. 1. The chemical composition and structure of the as-synthesised CuO/N-C-HNSs were analyzed by scanning electron microscopy (SEM), transmission electron microscopy (TEM), high-angle annular dark-field scanning transmission electron microscopy (HAADF-STEM), X-ray photoelectron spectroscopy (XPS) and powder X-ray diffraction (PXRD) analysis. The as-fabricated CuO/N-C-HNSs exhibited excellent catalytic performance towards C–H bond oxidation and a broad range of aromatic hydrocarbons were successfully oxidized into the corresponding products. Furthermore, the catalyst was easily recovered and recycled several times without a significant decrease in the catalytic activity.

2. Experimental details

2.1 Procedure for the C–H oxidation reaction

All the C–H oxidation reactions were performed in a 15 mL glass vial containing a magnetic needle. In a typical procedure, the reaction vial was charged with water (4 mL), a substrate (1 mmol) and a catalyst (20 mg). Then, 70% aqueous TBHP (1 mL) was added slowly using a glass syringe and the resulting mixture was stirred at room temperature (RT). The reaction vial was sealed and immersed in an oil bath. The oil bath temperature was increased from RT to 80 °C and maintained at 80 °C for 20 h. After 20 h, the reaction mixture was cooled at RT and transferred into a centrifuge tube. The catalyst was isolated by centrifugation and the homogeneous reaction mixture was mixed with 50 mL of water. The organic compounds were extracted using 90 mL ethyl acetate (30 mL each time). The combined organic layer was dried over sodium sulphate and finally evaporated to obtain the crude product. The crude

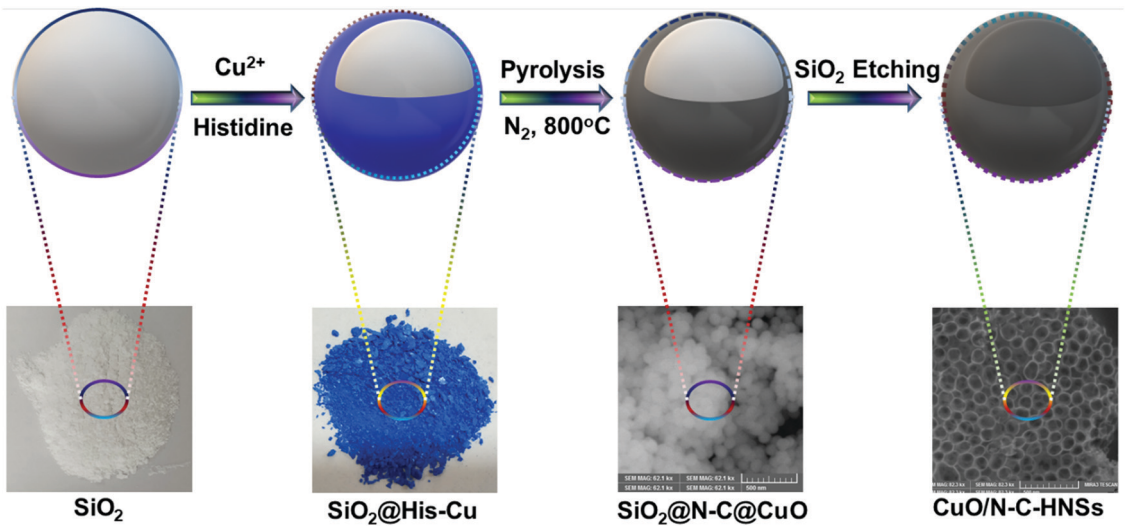

Fig. 1 Graphical representation of the synthesis of CuO/N-C-HNSs.

products were purified by column chromatography and the purified products were characterized by ^{1}H and ^{13}C nuclear magnetic resonance (NMR) spectroscopy.

3. Results and discussion

3.1 Catalyst characterization

The PXRD pattern of CuO/N-C-HNSs shows two broad diffraction peaks at 25° and 44° (Fig. 2), which are assigned to the reflections from (002) and (100) Bragg planes of graphitic carbon, respectively.[19,28,38] Thus, the XRD analysis confirms the formation of the graphitic carbon material. The peaks corresponding to CuO were not observed in the XRD spectra of CuO/N-C-HNSs; however, the XPS and HRTEM analyses confirmed that CuO species were indeed present in the material. The absence of XRD peaks corresponding to CuO could be possibly due to the amorphous nature or high dispersion of CuO nanoparticles in CuO/N-C-HNSs.[65]

To study the elemental composition and their oxidation states in CuO/N-C-HNSs, XPS analysis was performed (Fig. 3). The survey spectrum (Fig. 3a) confirmed the presence of Cu, N, C and O elements. The high-resolution Cu 2p spectrum (Fig. 3b) contains two peaks at 934.7 eV and 954.9 eV corresponding to Cu $2p_{3/2}$ and Cu $2p_{1/2}$, respectively. These binding energy peaks and the associated shakeup satellite peaks at 943.7 eV and 962.7 eV confirmed the presence of Cu^{2+} species.[66,67] The N 1s spectrum (Fig. 3c) was successfully deconvoluted into three peaks having binding energies of 398.2 eV, 399.7 eV and 402.4 eV, which were assigned to pyridinic N, graphitic N and N-oxide forms, respectively.[19] These differing nitrogen species anchored the CuO nanoparticles strongly and prevented their agglomeration and leaching during the catalytic reaction. The C 1s spectrum (Fig. 3d) was fitted with three peaks with binding energies of 284.4 eV, 285.9 eV and 288.7 eV, which were assigned to C–C, C–N and C═O, respectively, indicating the incorporation of heteroatoms into the as-fabricated nanocomposite.[38,65]

Structural and morphological characterizations of CuO/N-C-HNSs were conducted by electron microscopic analysis. The FE-SEM images (Fig. 4a and b) and TEM images (Fig. 4c and d) reveal that the CuO/N-C-HNS material possesses spherical morphology, which perfectly retains the size of the SiO_2 template (Fig. S1, ESI†). The hollow spherical structure arising from the etching of the SiO_2 template induces high porosity into the material and facilitates effective mass transport during the reaction. The HRTEM image (Fig. 4e) reveals the presence of finely dispersed CuO clusters having sizes below 10 nm in the CuO/N-C-HNS sample. The interplanar distance was measured to be 0.25 nm which is characteristic of the CuO (−111) crystal plane (Fig. 4f).[68] Next, the dispersion of CuO nanoparticles in CuO/N-C-HNSs was analyzed by HAADF-STEM imaging and mapping the various elements by using EELS (Fig. S2, ESI†). A number of finely dispersed bright dots corresponding to CuO species originated from the scattering of electrons by high density Cu atoms (Fig. S2a, ESI†). Moreover, the EELS elemental mapping reveals the uniform distribution of CuO and N over the entire carbon nanostructure. Thus, the SEM and TEM analyses confirm the formation of a hollow nanostructured material. The existence of finely dispersed CuO nanoparticles was confirmed by the HRTEM and XPS analyses.

The surface area and porosity of CuO/N-C-HNSs were determined by N_2 adsorption–desorption analysis (Fig. 5). The material exhibited a typical type (IV) isotherm with a hysteresis loop (Fig. 5a) which confirmed the existence of a mesoporous structure in the as-fabricated nanocomposite.[69] The pore-size distribution curve contains a peak centered at 4.3 nm (Fig. 5b). Due to the highly interconnected hollow nanostructure, the material possesses a large surface area of 372 $m^2\ g^{-1}$. Next, the copper content in CuO/N-C-HNSs was estimated to be 2.4 wt% by inductively coupled plasma-optical emission spectroscopy (ICP-OES) analysis. Thus, the outcomes of various characterization analyses confirm the successful formation of the CuO/N-C-HNS nanocomposite.

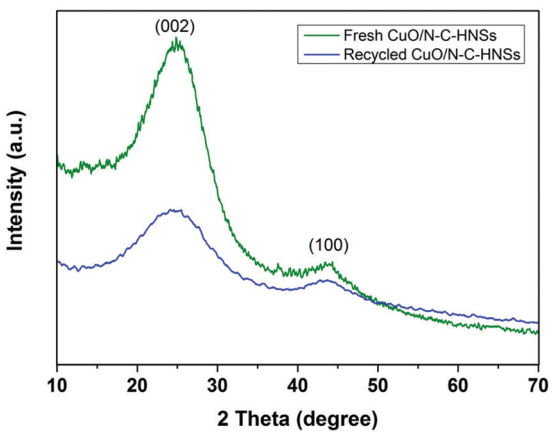

Fig. 2 XRD patterns of fresh and recycled CuO/N-C-HNSs.

3.2 Catalytic performance of CuO/N-C-HNSs towards C–H oxidation reactions

The catalytic performance of finely dispersed CuO/N-C-HNSs for the liquid phase oxidation of C–H bonds was evaluated using ethylbenzene as the model substrate and TBHP as the oxidizing agent (Table 1). In the beginning, the reaction was performed at 30 °C; however, only 18% conversion of ethylbenzene was observed with 61% selectivity towards the desired product acetophenone (Table 1, entry 1). The conversion and selectivity increased considerably when the reaction was carried out at 70 °C (Table 1, entry 2). Both the ethylbenzene conversion and acetophenone selectivity reached 99% when the reaction temperature was increased to 80 °C (Table 1, entry 3). However, increasing the reaction temperature further to 90 °C lowered the selectivity towards acetophenone to 97%, whereas the conversion of ethylbenzene remained unaffected (Table 1, entry 4). Therefore, the reaction temperature was kept constant at 80 °C for further optimization studies. Next, the effect of reaction time on conversion and selectivity in the oxidation of ethyl benzene was studied and the results are presented in Fig. S3 (ESI†). As shown in Fig. S3 (ESI†), the reaction provided constant conversion as well as selectivity towards the desired product after 20 h. Therefore, the reaction time was kept constant at 20 h for further studies. In comparison to

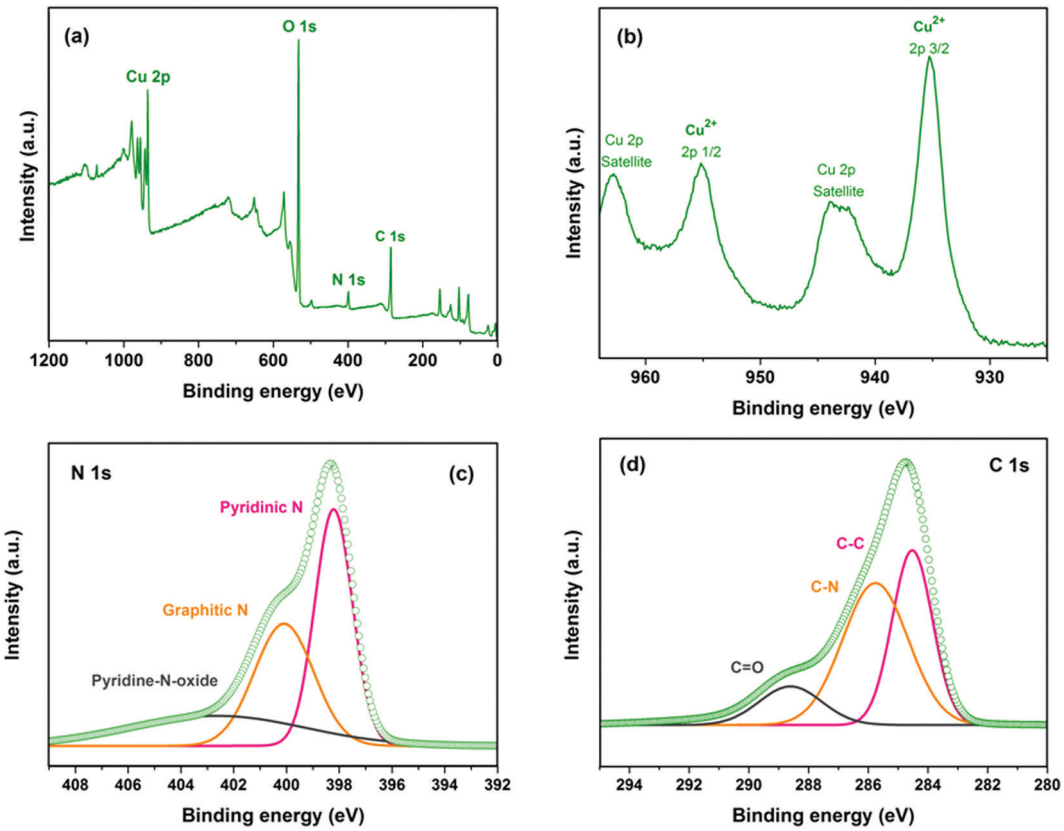

Fig. 3 XPS survey scan (a) and high-resolution scan of Cu 2p (b), N 1s (c) and C 1s (d) of CuO/N-C-HNSs.

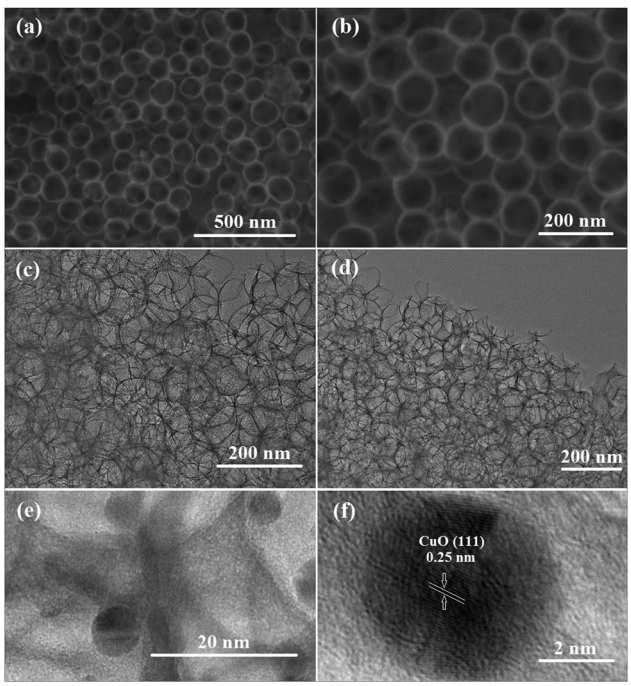

Fig. 4 FE-SEM images (a) and (b), TEM images (c) and (d) and HRTEM images (e) and (f) of CuO/N-C-HNSs.

CuO/N-C-HNSs, the nanomaterial CuO/C-HNSs without nitrogen doping provided only 67% conversion of ethylbenzene with 83% selectivity towards acetophenone. These results suggest that the nitrogen doping has a synergistic effect on the catalytic activity (Table 1, entry 5). The catalysts CuO powder, N-C-HNSs and activated carbon afforded ethylbenzene conversion of only 46%, 70% and 28%, respectively (Table 1, entries 6–8). A blank reaction, without any catalyst, provided only 8% conversion of ethylbenzene in 20 h (Table 1, entry 9) which indicates the poor rate of reaction for an uncatalyzed reaction. Next, other oxidizing agents such as molecular oxygen and hydrogen peroxide were also explored for the oxidation of ethylbenzene (Table 1, entries 10 & 11). However, both of them were unable to oxidize the ethylbenzene into acetophenone.

Next, the loading of CuO/N-C-HNSs on the liquid phase oxidation of ethylbenzene was studied (Table 1, entries 3, 12 & 13). Increasing the catalyst loading from 10 wt% to 20 wt% (with respect to ethylbenzene) increased both the conversion as well as selectivity towards the oxidation of ethylbenzene into acetophenone. The increase in conversion and selectivity can be attributed to the increased number of catalytically active sites available for the reaction resulting from the increased catalyst loading. However, increasing the catalyst loading further to 25 wt% did not increase the conversion or selectivity (Table 1, entry 14). These results reveal that the reaction with 20 wt% loading of CuO/N-C-HNSs affords an abundant number of active sites for the efficient conversion of ethylbenzene into acetophenone. All the C–H oxidation reactions were carried out using an excess quantity of TBHP (8 mmol) so that the reaction

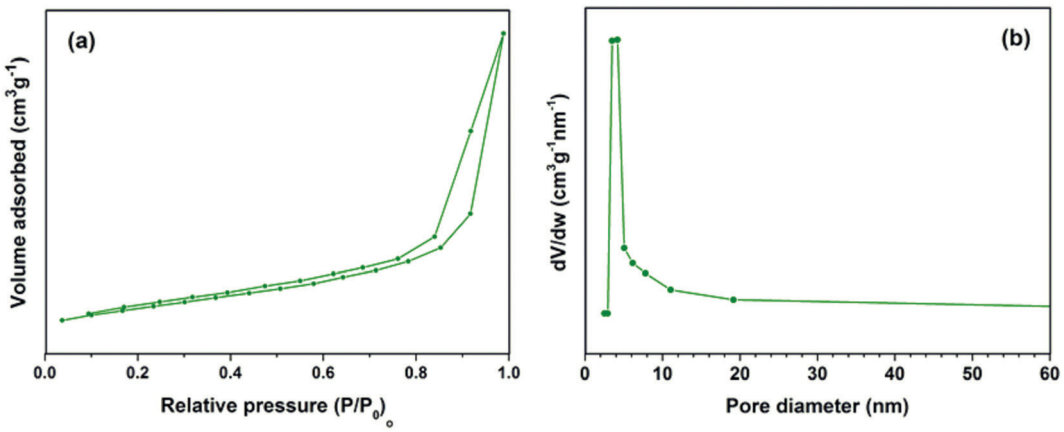

Fig. 5 Nitrogen adsorption–desorption isotherm (a) and the corresponding pore size distribution curve (b) of CuO/N-C-HNSs.

Table 1 Optimization of the reaction conditions for the oxidation of ethylbenzene[a]

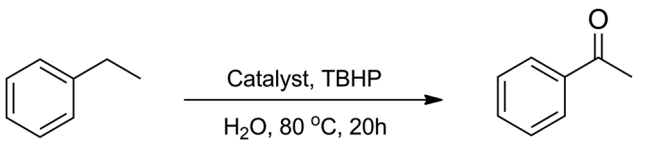

Entry	Catalyst	Temperature (°C)	Conversion[b] (%)	Selectivity[b] (%)	TOF (h^{-1})
1	CuO/N-C-HNSs	30	18	61	0.73
2	CuO/N-C-HNSs	70	74	77	3.77
3	CuO/N-C-HNSs	80	99	99	6.50
4	CuO/N-C-HNSs	90	99	97	6.34
5	CuO/C-HNSs	80	67	83	3.93
6	CuO powder	80	46	61	1.86
7	N-C-HNSs	80	70	77	3.58
8	Activated carbon	80	28	46	0.86
9	Blank	80	8	12	0.07
10[c]	CuO/N-C-HNSs	80	5	—	—
11[d]	CuO/N-C-HNSs	80	3	—	—
12[e]	CuO/N-C-HNSs	80	56	77	5.70
13[f]	CuO/N-C-HNSs	80	78	80	5.48
14[g]	CuO/N-C-HNSs	80	99	98	5.14
15[h]	CuO/N-C-HNSs	80	99	96	6.30
16[i]	CuO/N-C-HNSs	80	99	99	6.50

[a] Reaction conditions: ethylbenzene, 1 mmol; catalyst, 20 wt%; TBHP, 8 mmol; solvent, water (4 mL); time, 20 h. [b] Conversion and selectivity were determined by GC analysis. [c] Molecular oxygen. [d] H_2O_2. [e] Catalyst, 10 wt%. [f] Catalyst, 15 wt%. [g] Catalyst, 25 wt%. [h] TBHP, 2 mmol. [i] TBHP, 4 mmol.

follows first-order kinetics. However, to estimate the utilization efficiency of TBHP, the ethylbenzene oxidation was carried out by varying the quantity of TBHP (Table 1, entries 15 & 16). It was interesting to note that even with the reduced quantity of TBHP (2 mmol) the conversion of ethylbenzene could still reach 99% with an acetophenone selectivity of 96% (Table 1, entry 15).

To further demonstrate the wide applicability of CuO/N-C-HNSs, the selective oxidation of various substituted aromatic hydrocarbons was carried out using the optimized reaction parameters. As shown in Table 2, a variety of substituted ethylbenzenes were smoothly converted into the corresponding ketones with high conversion and selectivity values. Propylbenzene behaved similarly to ethylbenzene and provided comparable conversion as well as selectivity (Table 2, entries 1 & 4). Bulky substrates such as diphenylmethane and fluorene could also be smoothly oxidized into the corresponding ketones with excellent conversion and selectivity (Table 2, entries 6 & 8). Fluorene was found to be insoluble in water; therefore, the oxidation of fluorene was carried out in dimethyl sulfoxide solvent, while the other reaction parameters were

Table 2 Oxidation of various substituted aromatic hydrocarbons into corresponding ketones[a]

Entry	Substrate	Product	Conversion[b] (%)	Selectivity[b] (%)
1			99	99
2	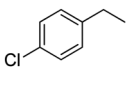	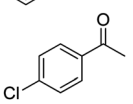	94	95
3	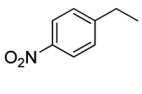	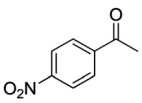	87	91
4	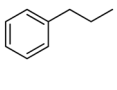	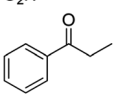	93	95
5			90	84
6	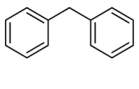	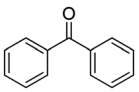	99	99
7	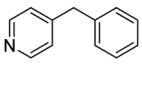	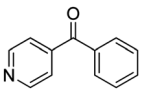	92	93
8[c]	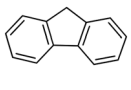	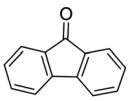	95	97

[a] Reaction conditions: ethylbenzene, 1 mmol; catalyst, 20 wt%; TBHP, 8 mmol; solvent, water (4 mL); time, 20 h. [b] Conversion and selectivity were determined by GC analysis. [c] Solvent, DMSO (4 mL).

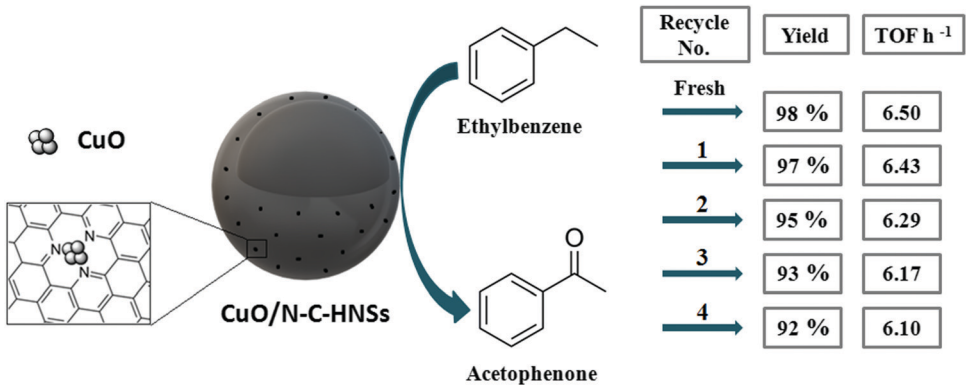

Fig. 6 Reusability of CuO/N-C-HNSs in the oxidation of ethylbenzene.

kept constant. The C–H oxidation in the heteroaromatic substrate 4-benzylpyridine was also achieved with high conversion as well as selectivity (Table 2, entry 7). Thus, the as-fabricated novel nanocomposite, CuO/N-C-HNSs, demonstrates excellent catalytic activity and versatility towards selective oxidation of aromatic hydrocarbons.

The stability and recyclability of a catalyst in heterogeneous catalysis make the process sustainable for commercial applications.[70] Thus, the stability as well as recyclability of the CuO/N-C-HNS catalyst was examined. The recyclability of the catalyst was investigated in the oxidation of ethylbenzene into acetophenone. As shown in Fig. 6, the CuO/N-C-HNSs were recycled four times without considerable loss in their catalytic activity. The ICP-OES analysis of the reaction mixture after isolating the catalyst shows the absence of copper which indicates that the CuO nanoparticles remain firmly anchored on N-C-HNSs during the reactions. Moreover, the HRTEM image (Fig. S4, ESI†) of CuO/N-C-HNSs recycled four times shows a similar particle size of the CuO nanoparticles to that of the fresh catalyst and no agglomeration of CuO nanoparticles was observed. Additionally, the PXRD analysis of the CuO/N-C-HNS catalyst reused four times shows an XRD pattern similar to that of the fresh sample (Fig. 2). The heterogeneity of CuO/N-C-HNSs was examined by a hot filtration test in which the catalyst was isolated from the reaction mixture after 4 h by simple filtration and the reaction was further continued without the catalyst. There was no further reaction in the filtrate after removal of the catalyst suggesting the heterogeneous nature of CuO/N-C-HNSs. Thus, these results demonstrate the excellent stability as well as recyclability of the finely dispersed CuO/N-C-HNS catalyst.

4. Conclusions

By using SiO_2 nanospheres as the sacrificial template, we have successfully fabricated finely dispersed CuO/N-C-HNSs which exhibit excellent catalytic activity and selectivity towards the liquid phase oxidation of sp^3 C–H bonds in aromatic hydrocarbons using TBHP as the oxidizing agent and water as the green solvent. Nitrogen-doping facilitates the dispersion of CuO in the form of nanoparticles having particle sizes below 10 nm. Additionally, the strong metal–support interaction arising from the nitrogen doping prevents the aggregation as well as leaching of the CuO nanoparticles during the reaction. The efficient conversion of a wide variety of aromatic hydrocarbons into the corresponding ketones demonstrates the versatility of CuO/N-C-HNSs in the C–H oxidation reaction. Moreover, the CuO/N-C-HNSs can be easily isolated and recycled several times without significant loss in their catalytic activity.

Conflicts of interest

There are no conflicts to declare.

Acknowledgements

The authors sincerely acknowledge the Godrej Industries Limited, India and J. C. Bose Fellowship, SERB-DST, GoI for providing the financial support.

References

1 S. Fan, W. Dong, X. Huang, H. Gao, J. Wang, Z. Jin, J. Tang and G. Wang, *ACS Catal.*, 2017, **7**, 243–249.
2 E. Gaster, S. Kozuch and D. Pappo, *Angew. Chem., Int. Ed.*, 2017, **56**, 5912–5915.
3 Z. Guo, B. Liu, Q. Zhang, W. Deng, Y. Wang and Y. Yang, *Chem. Soc. Rev.*, 2014, **43**, 3480.
4 J. Liu, X. Zhang, H. Yi, C. Liu, R. Liu, H. Zhang, K. Zhuo and A. Lei, *Angew. Chem., Int. Ed.*, 2015, **54**, 1261–1265.
5 Y. Chen, X. Huang, X. Feng, J. Li, Y. Huang, J. Zhao, Y. Guo, X. Dong, R. Han, P. Qi, Y. Han, H. Li, C. Hu and B. Wang, *Chem. Commun.*, 2014, **50**, 8374–8377.
6 L. Wang, Y. Zhu, J.-Q. Wang, F. Liu, J. Huang, X. Meng, J.-M. Basset, Y. Han and F.-S. Xiao, *Nat. Commun.*, 2015, **6**, 6957.
7 Y. Hirai, T. Kojima, Y. Mizutani, Y. Shiota, K. Yoshizawa and S. Fukuzumi, *Angew. Chem., Int. Ed.*, 2008, **47**, 5772–5776.

8 D. Deng, Y. Yang, Y. Gong, Y. Li, X. Xu and Y. Wang, *Green Chem.*, 2013, **15**, 2525.
9 A. V. Biradar and T. Asefa, *Appl. Catal., A*, 2012, **435–436**, 19–26.
10 R. Xie, G. Fan, L. Yang and F. Li, *ChemCatChem*, 2016, **8**, 363–371.
11 Y. Kuwahara, Y. Yoshimura and H. Yamashita, *Catal. Sci. Technol.*, 2016, **6**, 442–448.
12 Y. Kuwahara, Y. Yoshimura and H. Yamashita, *Dalton Trans.*, 2017, **46**, 8415–8421.
13 J. Luo, F. Peng, H. Yu, H. Wang and W. Zheng, *ChemCatChem*, 2013, **5**, 1578–1586.
14 P. Patel, S. Nandi, T. Menapara, A. V. Biradar, R. K. Nagarale, N. H. Khan and R. I. Kureshy, *Appl. Catal., A*, 2018, **565**, 127–134.
15 C. K. P. Neeli, A. Narani, R. K. Marella, K. S. Rama Rao and D. R. Burri, *Catal. Commun.*, 2013, **39**, 5–9.
16 S. J. Singh and R. V. Jayaram, *Catal. Commun.*, 2009, **10**, 2004–2007.
17 S. J. Singh and R. V. Jayaram, *Synth. Commun.*, 2012, **42**, 299–308.
18 A. S. Burange, S. R. Kale and R. V. Jayaram, *Tetrahedron Lett.*, 2012, **53**, 2989–2992.
19 D. A. Bulushev, A. L. Chuvilin, V. I. Sobolev, S. G. Stolyarova, Y. V. Shubin, I. P. Asanov, A. V. Ishchenko, G. Magnani, M. Riccò, A. V. Okotrub and L. G. Bulusheva, *J. Mater. Chem. A*, 2017, **5**, 10574–10583.
20 Z. Jin, C. Liu, K. Qi and X. Cui, *Sci. Rep.*, 2017, **7**, 39695.
21 H. Chen, K. Shen, Q. Mao, J. Chen and Y. Li, *ACS Catal.*, 2018, **8**, 1417–1426.
22 J. Zhao, X. Quan, S. Chen, Y. Liu and H. Yu, *ACS Appl. Mater. Interfaces*, 2017, **9**, 28685–28694.
23 H. Park, S. Oh, S. Lee, S. Choi and M. Oh, *Appl. Catal., B*, 2019, **246**, 322–329.
24 M. Kuang, Q. Wang, P. Han and G. Zheng, *Adv. Energy Mater.*, 2017, **7**, 1700193.
25 Z. Chen, R. Wu, Y. Liu, Y. Ha, Y. Guo, D. Sun, M. Liu and F. Fang, *Adv. Mater.*, 2018, **30**, 1802011.
26 W. Gong, Y. Lin, C. Chen, M. Al-Mamun, H. Lu, G. Wang, H. Zhang and H. Zhao, *Adv. Mater.*, 2019, **31**, 1808341.
27 D. Ding, K. Shen, X. Chen, H. Chen, J. Chen, T. Fan, R. Wu and Y. Li, *ACS Catal.*, 2018, **8**, 7879–7888.
28 W. Zang, T. Yang, H. Zou, S. Xi, H. Zhang, X. Liu, Z. Kou, Y. Du, Y. P. Feng, L. Shen, L. Duan, J. Wang and S. J. Pennycook, *ACS Catal.*, 2019, **9**, 10166–10173.
29 W. Li, C. Min, F. Tan, Z. Li, B. Zhang, R. Si, M. Xu, W. Liu, L. Zhou, Q. Wei, Y. Zhang and X. Yang, *ACS Nano*, 2019, **13**, 3177–3187.
30 D. Karapinar, N. T. Huan, N. Ranjbar Sahraie, J. Li, D. Wakerley, N. Touati, S. Zanna, D. Taverna, L. H. Galvão Tizei, A. Zitolo, F. Jaouen, V. Mougel and M. Fontecave, *Angew. Chem., Int. Ed.*, 2019, **58**, 15098–15103.
31 J. Xie, J. D. Kammert, N. Kaylor, J. W. Zheng, E. Choi, H. N. Pham, X. Sang, E. Stavitski, K. Attenkofer, R. R. Unocic, A. K. Datye and R. J. Davis, *ACS Catal.*, 2018, **8**, 3875–3884.
32 X. Han, X. Ling, Y. Wang, T. Ma, C. Zhong, W. Hu and Y. Deng, *Angew. Chem., Int. Ed.*, 2019, **58**, 5359–5364.
33 B.-H. Lee, S. Park, M. Kim, A. K. Sinha, S. C. Lee, E. Jung, W. J. Chang, K.-S. Lee, J. H. Kim, S.-P. Cho, H. Kim, K. T. Nam and T. Hyeon, *Nat. Mater.*, 2019, **18**, 620–626.
34 X. Fang, Q. Shang, Y. Wang, L. Jiao, T. Yao, Y. Li, Q. Zhang, Y. Luo and H.-L. Jiang, *Adv. Mater.*, 2018, **30**, 1705112.
35 L. Liu, U. Díaz, R. Arenal, G. Agostini, P. Concepción and A. Corma, *Nat. Mater.*, 2017, **16**, 132–138.
36 P. Xie, T. Pu, A. Nie, S. Hwang, S. C. Purdy, W. Yu, D. Su, J. T. Miller and C. Wang, *ACS Catal.*, 2018, **8**, 4044–4048.
37 A. K. Kar and R. Srivastava, *ACS Sustainable Chem. Eng.*, 2019, **7**, 13136–13147.
38 Y. Chen, Z. Li, Y. Zhu, D. Sun, X. Liu, L. Xu and Y. Tang, *Adv. Mater.*, 2019, **31**, 1806312.
39 X.-H. Li, J.-S. Chen, X. Wang, J. Sun and M. Antonietti, *J. Am. Chem. Soc.*, 2011, **133**, 8074–8077.
40 Y. Gao, G. Hu, J. Zhong, Z. Shi, Y. Zhu, D. S. Su, J. Wang, X. Bao and D. Ma, *Angew. Chem., Int. Ed.*, 2013, **52**, 2109–2113.
41 P. Zhang, Y. Gong, H. Li, Z. Chen and Y. Wang, *Nat. Commun.*, 2013, **4**, 1593.
42 X. Lin, Z. Nie, L. Zhang, S. Mei, Y. Chen, B. Zhang, R. Zhu and Z. Liu, *Green Chem.*, 2017, **19**, 2164–2173.
43 X. Lin, S. Zhao, Y. Chen, L. Fu, R. Zhu and Z. Liu, *J. Mol. Catal. A: Chem.*, 2016, **420**, 11–17.
44 Y. Qiu, C. Yang, J. Huo and Z. Liu, *J. Mol. Catal. A: Chem.*, 2016, **424**, 276–282.
45 X. Lin, S. Jie and Z. Liu, *Mol. Catal.*, 2018, **455**, 143–149.
46 S. Nie, J. Wang, X. Huang, X. Niu, L. Zhu and X. Yao, *ACS Appl. Nano Mater.*, 2018, **1**, 6567–6574.
47 S. Pendem, R. Singuru, C. Sarkar, B. Joseph, J.-F. Lee, D. B. Shinde, Z. Lai and J. Mondal, *ACS Appl. Nano Mater.*, 2018, **1**, 4836–4851.
48 R. Nie, J. Chen, M. Chen, Z. Qi, T.-W. Goh, T. Ma, L. Zhou, Y. Pei and W. Huang, *Green Chem.*, 2019, **21**, 1461–1466.
49 L. Zhang, S. Jie, N. Cheng and Z. Liu, *ACS Sustainable Chem. Eng.*, 2019, **7**, 19474–19482.
50 L. Zhang, S. Jie and Z. Liu, *New J. Chem.*, 2019, **43**, 7275–7281.
51 W. Liu, L. Zhang, X. Liu, X. Liu, X. Yang, S. Miao, W. Wang, A. Wang and T. Zhang, *J. Am. Chem. Soc.*, 2017, **139**, 10790–10798.
52 J. Luo, H. Yu, H. Wang and F. Peng, *Catal. Commun.*, 2014, **51**, 77–81.
53 S. Huang, Y. Zhao and R. Tang, *RSC Adv.*, 2016, **6**, 90887–90896.
54 W.-F. Xu, W.-J. Chen, D.-C. Li, B.-H. Cheng and H. Jiang, *Ind. Eng. Chem. Res.*, 2019, **58**, 3969–3977.
55 X. Hu, Y. Liu, H. Huang, B. Huang, G. Chai and Z. Xie, *Green Chem.*, 2020, **22**, 1291–1300.
56 X. Hu, X. Sun, Q. Song, Y. Zhu, Y. Long and Z. Dong, *Green Chem.*, 2020, **22**, 742–752.
57 S. Yang, L. Peng, P. Huang, X. Wang, Y. Sun, C. Cao and W. Song, *Angew. Chem., Int. Ed.*, 2016, **55**, 4016–4020.
58 Y. Qin, H. Guo, B. Wang, J. Li, R. Gao, P. Qiu, M. Sun and L. Chen, *Chem. – Asian J.*, 2019, **14**, 1535–1540.
59 Y. Su, Y. Li, Z. Chen, J. Huang, H. Wang, H. Yu, Y. Cao and F. Peng, *ChemCatChem*, 2021, **13**, 646–655.

60 D. K. Kim, S. Bong, X. Jin, K. Seong, M. Hwang, N. D. Kim, N.-H. You and Y. Piao, *ACS Appl. Mater. Interfaces*, 2019, **11**, 1996–2005.
61 C. Hu and L. Dai, *Adv. Mater.*, 2019, **31**, 1804672.
62 Z. Liu, H. Nie, Z. Yang, J. Zhang, Z. Jin, Y. Lu, Z. Xiao and S. Huang, *Nanoscale*, 2013, **5**, 3283.
63 S. Yang, L. Zhi, K. Tang, X. Feng, J. Maier and K. Müllen, *Adv. Funct. Mater.*, 2012, **22**, 3634–3640.
64 Z. Huang, H. Pan, W. Yang, H. Zhou, N. Gao, C. Fu, S. Li, H. Li and Y. Kuang, *ACS Nano*, 2018, **12**, 208–216.
65 S. S. R. Gupta, A. Vinu and M. L. Kantam, *ChemPlusChem*, 2021, **86**, 259–269.
66 S. S. R. Gupta and M. L. Kantam, *Catal. Today*, 2018, **309**, 189–194.
67 S. S. R. Gupta, A. V. Nakhate, G. P. Deshmukh, S. Periasamy, P. S. Samudrala, S. K. Bhargava and M. Lakshmi Kantam, *ChemistrySelect*, 2018, **3**, 8436–8443.
68 S. S. R. Gupta, A. Vinu and M. L. Kantam, *J. Catal.*, 2020, **389**, 259–269.
69 S. S. R. Gupta, A. V. Nakhate, K. B. Rasal, G. P. Deshmukh and L. K. Mannepalli, *New J. Chem.*, 2017, **41**, 15268–15276.
70 S. S. R. Gupta and M. L. Kantam, *Catal. Commun.*, 2019, **124**, 62–66.

